A new magnet design for future Kibble balances

Shisong Li[1]*, Michael Stock[1]†, Stephan Schlamminger[2,3]‡

1. Bureau international des poids et mesures (BIPM), F-92312 Sèvres, France
2. National Institute of Standards and Technology (NIST), Gaithersburg, MD 20899, USA
3. Ostbayerische Technische Hochschule (OTH) Regensburg, 93053 Regensburg, Germany

Abstract

We propose a new permanent magnet system for Kibble balance experiments, which combines advantages of the magnet designs invented by the National Physical Laboratory (NPL) and by the Bureau International des Poids et Mesures (BIPM). The goal of the proposed magnet system is to minimize the coil-current effect and to optimize the shielding at the same time. In the proposed design, a permanent magnet system with two gaps, each housing a coil, is employed to minimize the coil current effect, by reducing the linear coil-current dependence reported for the single air gap design by at least one order of magnitude. Both air gaps of the magnet are completely surrounded by high-permeability material, and hence the coils are shielded from outside magnetic fields and no magnetic field leaks outside of the magnet system. An example of the new magnet system is given and the analysis shows that the magnetic field in the air gap can be optimized to meet the requirement to be used in Kibble balances.

Submitted to: *Metrologia*
February 10, 2021

*leeshisong@sina.com
†mstock@bipm.org
‡stephan.schlamminger@nist.gov

1 Introduction

Several Kibble balances, formerly known as watt balances [1], are operational or are under construction at National Metrology Institutes (NMIs) around the world [2–11]. As of 2017, the Kibble balance was used to measure the Planck constant, h, and in the future, will be employed to realize the unit of mass, i.e., kilogram, in a revised international system of units (SI). The purpose of the Kibble balance is to establish a link between classical and quantum mechanics [12], so that the kilogram can be derived from measurements of quantities that do not rely on artefact standards, but instead are traced to high accuracy standards for length, time, voltage, and resistance. The principle and operation of a Kibble balance can be found elsewhere, for example, [13].

The magnet is one of the most important elements in a Kibble balance. In past decades, many different coil and magnet systems were designed and have been used to measure the Planck constant h [9, 14–19]. Among these systems, a permanent magnet with air gap(s) displayed significant advantages and has been widely employed in Kibble balances. One well-known design, shown in figure 1(a), was proposed by the Kibble balance group at the Bureau international des poids et mesures (BIPM) [16], which has been implemented in several Kibble balance experiments [5, 10, 11, 19, 20]. The BIPM-type magnet can generate a strong, uniform magnetic field at the coil position with a compact design. Since the air gap and the coil are surrounded by high-permeability yokes, it has good shielding properties.

However, a recent theoretical and experimental study based on the BIPM magnet showed the magnetic profile of such a magnet can be significantly sloped by the coil-current, and this profile change may cause a considerable systematic bias in the measurement [21]. This conclusion prompted us to re-evaluate the existing Kibble balance magnets and try to find a better magnet design that can suppress the coil-current effect without any compensation or correction. Ideally, the improved design should not change the main advantages of the existing magnet designs, e.g. field strength, field uniformity, shielding, etc. Here, a novel magnet design, that meets the magnetic properties of the BIPM design, without the current induced slope, is proposed.

Section 2 gives a brief summary of different magnet designs and their related coil-current effect. In section 3, the new design is presented, and several different optimizations are discussed in order to achieve a more uniform field in the coil moving region.

2 Coil current effect of existing Kibble balance magnets

While it is in principle possible to use an electromagnet in a Kibble balance, this practice has declined in recent years. The third generation Kibble balance at the National Institute of Standards and Technology (NIST, USA) [14] used a superconducting coil. A flat profile was generated by using multiple coils. The high cost and effort to keep the coils at liquid helium temperatures outweigh the advantage of having a calculable field profile. In the new generation Kibble balance, NIST-4, the BIPM-type permanent magnet was chosen to replace the superconducting coil system [19]. Researchers working on the joule balance at the National Institute of Metrology (NIM, China) also chose to use an electromagnet. In the beginning, conventional coils were used and the heating of the coil during weighing became the main limitation on forces of the order of a Newton [22]. The conventional coil was subsequently replaced by an electromagnet with an iron yoke [23], reducing the heating effect because of

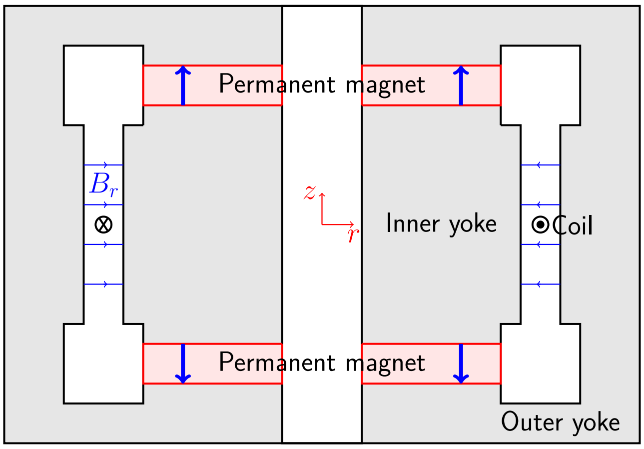

(a)

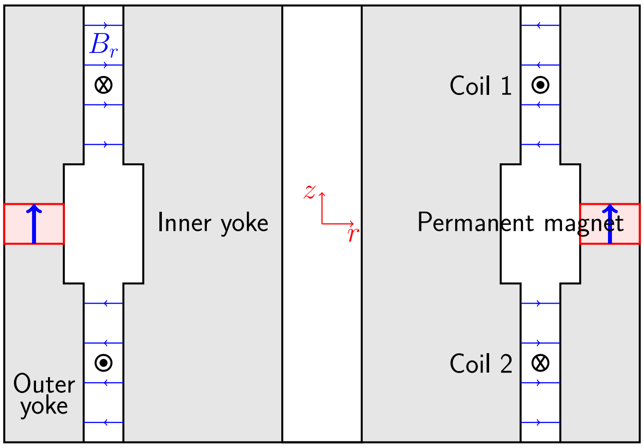

(b)

Figure 1: The construction of two typical Kibble balance magnets: (a) BIPM-type and (b) NPL-type. Both the NPL-type and the BIPM-type magnets are upside-down symmetrical with respect to a horizontal plane in the middle of the magnet. The flux of permanent magnets is guided by high permeability yokes to the coil(s). The NPL-type magnet has two radial air gaps, and the magnetic flux in these two gaps is in an opposite direction (radial). Two coils in opposite polarity are used to generate an upward or downward magnetic force. The BIPM-type design employs two permanent magnets, with opposite poles facing each other. This design has only one radial air gap and only one coil is required.

the larger flux density. However, time-dependent external magnetic flux generated in the laboratory changed the main field produced by the electromagnet at the 10^{-7} level [8]. Now, the joule balance uses a BIPM-type magnet [20].

Currently, all Kibble balances around the world employ permanent magnet systems. The construction of these magnet systems can be broadly categorized into two different types, based on the number of air gaps and coils that are used. The BIPM type magnet has one gap and requires one coil, which we abbreviate as OGOC (one-gap, one-coil) structure. The NPL magnet, on the other hand, has two air gaps and requires two coils, although both coils are wound on one former. This design is referred to as TGTC (two-gaps, two-coils) structure. So far, only the NPL-NRC system shown in figure 1(b), which was originally built in the National Physical Laboratory (NPL, UK) and has been moved to the National Research Council (NRC, Canada) in 2009, uses the TGTC structure, and all the other Kibble balances use an OGOC

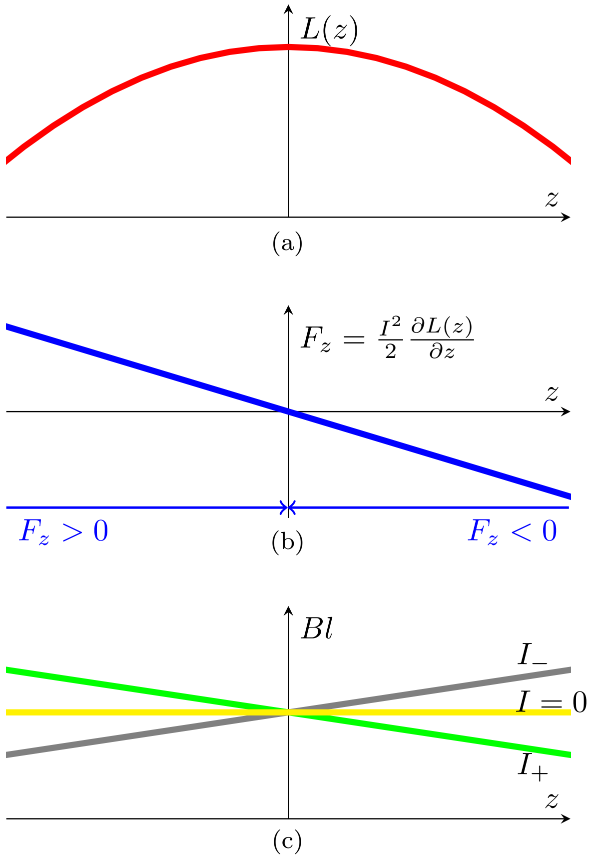

Figure 2: The DC inductance of the coil L, the inductance force F_z, and the magnetic profile $Bl(I)$ as functions of the vertical position z of the coil. At the magnetic centre ($z = z_0$), L has the maximum value while $F_z = 0$. When the coil is above or below z_0, the inductance force will point to z_0 and pull the coil back to the centre.

design (but not all use a BIPM type magnet design).

One important property of the permanent magnet system is how the permanent magnetic field will be affected by the coil current in the weighing measurement, i.e., the coil-current effect. Using the magnetic equation given in [15], the geometric factor (flux density integrated along the coil) with the current present, $(Bl)_w$ is given by

$$(Bl)_w = (Bl)_v(1 + \alpha I + \beta I^2), \tag{1}$$

where $(Bl)_v$ is the geometrical factor without current in the coil, α, β the linear and nonlinear coefficients, and I the coil current. In the original Kibble balance experiment, the $(Bl)_w$ is determined by weighing and the $(Bl)_v$ during the velocity phase. Both, experimental results and theoretical analysis show that the quadratic dependence of the geometric factor on the current can be made negligible in symmetric magnet designs [24–27]. However, the experimenters should take care of the potential bias from the linear term. It has been shown in [21] that the linear term is mainly caused by the inductive energy change of the current-carrying coil, written as

$$\alpha = \frac{1}{2(Bl)_v}\frac{\partial L}{\partial z}, \tag{2}$$

where L is the coil's inductance at low frequencies.

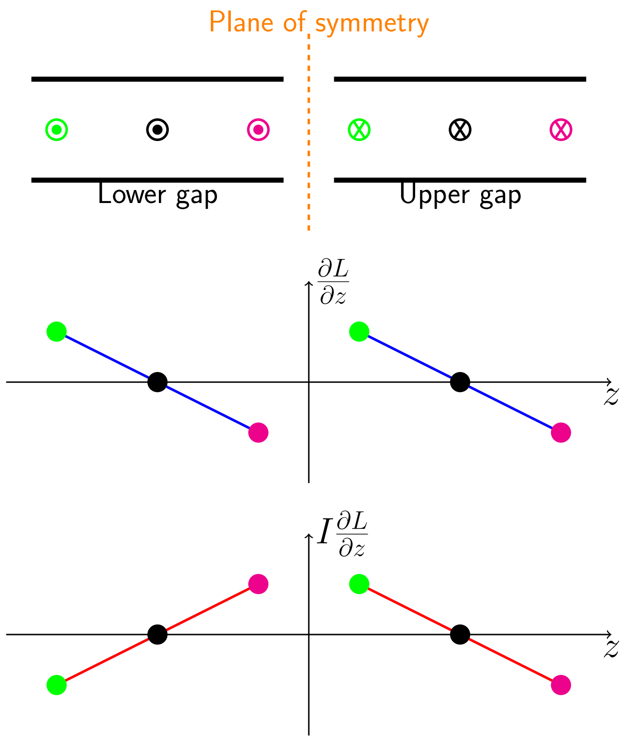

Figure 3: The magnetic profile change due to coil current in TGTC magnet systems. The top diagram depicts the two physically and electrically (in series opposition) connected coils in the two gaps. The middle graph shows the $\partial L/\partial z$ for both coils. The lower graph shows $I_+(\partial L/\partial z)$ for both coils, in which the current has opposite signs. Three colours shown in the plot denote three different coil positions.

Experimental measurements (e.g., [19, 21]) show that for a typical magnet configuration, L is a quadratic function of coil position z (shown in figure 2). Based on the virtual energy principle, the inductance force of the coil,

$$F_z = \frac{I^2}{2}\frac{\partial L}{\partial z}, \tag{3}$$

has a positive sign with $z < 0$ and a negative sign with $z > 0$. As a result, the reluctance force F_z always tries to pull the coil toward the centre of the air gap independent of the sign of the current in the coil.

From the known α, a linear function of coil position z, the Bl produced by this effect for the current carrying coil in force mode can be calculated by simply multiplying α with I_+ for the mass-on and I_- for the mass-off measurements. The results are the two linear curves shown in the bottom plot of figure 2. Experimental measurements on the BIPM magnet provide evidence for this theory. The magnetic profile became significantly sloped by the coil current. For the BIPM case, with $I = \pm 13.33\,\mathrm{mA}$, the change of $Bl(I_+)$ and $Bl(I_-)$ is about $\mp 2\times 10^{-4}$ in 10 mm.

One major disadvantage of the sloped magnetic profiles is that the measurement result will be sensitive to changes of the vertical coil position between the mass-on and mass-off measurements [21]. The relative size of the effect is about $1 \times 10^{-8}\,\mu\mathrm{m}^{-1}$ for the BIPM Kibble balance. For a Kibble balance with a µm change of the coil position during mass-on and mass-off, it will generate a bias of order 10^{-8}. Although the bias introduced by this effect can be corrected, it is better to reduce the coefficient by a factor of 10, to about $1 \times 10^{-9}\,\mu\mathrm{m}^{-1}$.

We noticed that in the TGTC design, currently implemented in the NPL-type magnet, because two coils of opposite currents are used, the magnetic field change due to the linear term for the combined coil cancels and $\alpha \approx 0$. The diagram shown in figure 3 gives a simple explaination: The two coils in the two gaps are shown in the top diagram. The middle diagram shows the $\partial L/\partial z$ for each coil. Due to the symmetry of the magnet, the partial derivative of the inductance of each coil versus z has the same dependence on the relative coil position. The derivatives are identical, but translated by the vertical separation of the gaps. The coils are connected electrically in series opposition, i.e., in one coil circulates clockwise and the other counterclockwise. Hence, in the product of $I(\partial L/\partial z)$, one expression flips the sign with respect to the other. The sum of both effects $I(\partial L_1/\partial z) - I(\partial L_2/\partial z)$ is eliminated.

The published measurements of the NPL-NRC and NIST Kibble balances verify this analysis: the α value of the NPL-NRC magnet is measured as $2 \times 10^{-7}\,\mathrm{mA}^{-1}$ [15] and the NIST-4 (BIPM-type) calibrated α is $-2.35 \times 10^{-6}\,\mathrm{mA}^{-1}$ [26]. By using the TGTC magnet, the linear coefficient has been reduced by about one order of magnitude.

As shown above, the NPL-type magnet design is a good option to reduce the effect of the coil current on the shape of the magnetic field. The NPL magnet design has two weaknesses, which both reduce the shielding of the coil from external magnetic fields. First, the SmCo (permanent magnet) is part of the outer yoke, allowing external flux lines to cross into the SmCo and ultimately into the yoke. Second, the open gaps allow external flux to enter the yoke. Every surface in the outer yoke that allows magnetic flux to couple into the magnet will also provide an opportunity for magnetic flux from the permanent magnet to escape. The open gaps at the top and bottom of the magnet are especially troublesome. The magnetic flux density above the NPL magnet is high and is a cause for concern with respect to the magnetic forces on the masses that have non-negligible susceptibility [28]. While the SmCo can be easily moved into the inner yoke, shielding the air gaps requires a more substantial redesign. The design presented in the next section combines the rejection of the coil current effect of the TCTG design with near perfect shielding.

3 Design of the new magnet

The proposed Kibble balance magnet design is shown in figure 4(a). Two permanent magnets are used, and the major magnetic flux of each permanent magnet goes through an individual air gap formed by high permeability yokes. Since the North pole of one magnet faces the South pole of the other, the flux direction at the two air gaps is opposite along the radial direction. Two coils, wired in series opposition, similar to the NPL-type design are used in this design.

The upper and lower magnetic circuits are connected on the outside by the yoke and on the inside by non-magnetic materials. The continuous yoke on the outside provides near perfect shielding of the magnet system. In the centre section, the yoke can be made thinner than at the top and bottom of the magnet, because the yoke caries much less flux density. The separation in the inner yoke introduces a large magnetic resistance between the upper and lower magnetic circuits to control the reduction of the magnetic flux in the air gap. Aluminum or a combination of an aluminum space and air can be used to form the separation. A clever design may allow space for the spider that holds the upper and lower coil.

The magnetic field in the air gap depends on the dimension of the non-magnetic material. Due to a symmetrical structure, the same amount of magnetic flux ϕ is going through the two air gaps in the opposite direction. The magnetic flux traversing the non-magnetic material is

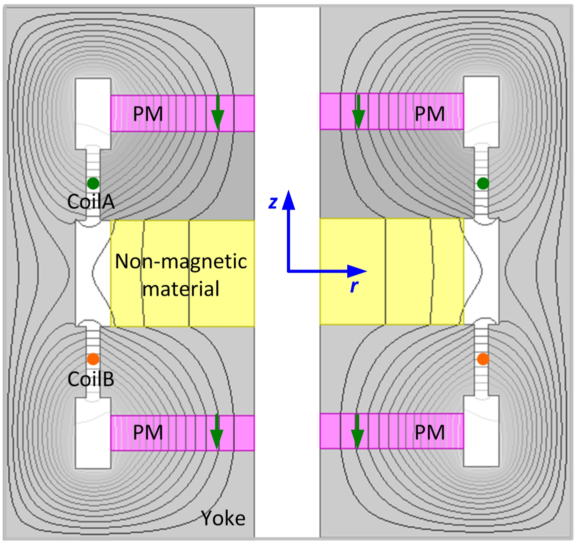

(a)

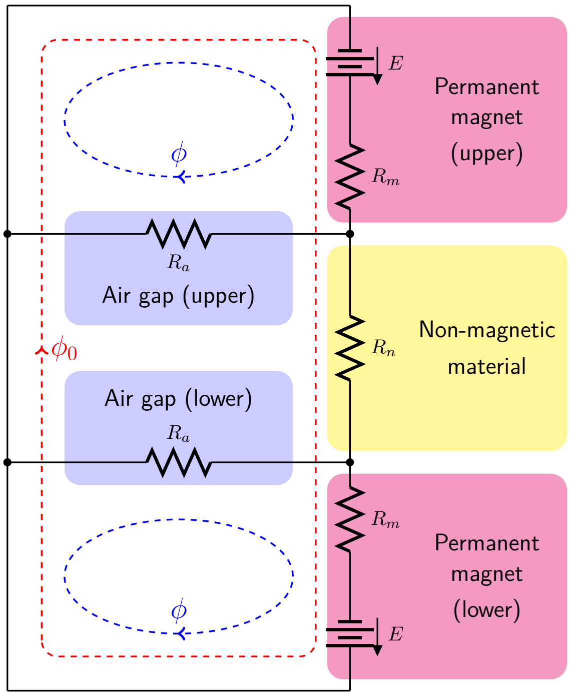

(b)

Figure 4: (a) The structure of the proposed Kibble balance magnet. PM denotes permanent magnets and the arrow shows the magnetic flux direction. (b) An equivalent electrical circuit of the proposed magnet construction by Hopkinson's law. The magnetic reluctance is proportional to the length along the flux direction, and inversely proportional to the permeability and the area allowing the flux to go through. E is proportional to the height of the permanent magnet ring.

labelled ϕ_0. For the lower or upper magnetic circuit,

$$(R_a + R_m)\phi + R_n\phi_0 = E, \tag{4}$$

where R_a, R_m denote the magnetic reluctances of each air gap and each permanent magnet, R_n the magnetic reluctance of the non-magnetic material, E the magnetomotive force (mmf) of each permanent magnet. As shown in figure 4(b), the equation above is derived from Hopkinson's law the magnetic equivalent of Ohm's law. Applying Hopkinson's law to the path through the non-magnetic material and two permanent magnets yields

$$2(\phi + \phi_0)R_m + \phi_0 R_n = 2E. \tag{5}$$

A combination of equations (4) and (5) yields the flux through each air gap as

$$\phi = \frac{E}{R_m\left(\frac{R_a}{R_n} + 1\right) + R_a\left(\frac{R_m}{R_n} + 1\right)}. \tag{6}$$

According to equation (6), the magnetic field in the air gap is related to the magnetic reluctance of the non-magnetic material. In order to keep the majority of the flux in the air gap, the magnetic reluctance of the non magnetic spacer has to be much larger than the reluctance of the permanent magnet ($R_n >> R_m$) and the reluctance of the air gap ($R_n >> R_a$). It is easy to see when, R_n is much larger than R_m since both regions are cylinders with the same radius and similar magnetic permeability of about one. Hence, the ratio of the two reluctances is given by the ratios of the heights, $R_n/R_m = h_n/h_m$. To fulfil $R_n >> R_m$, the nonmagnetic spacer needs to be taller than each permanent magnet. The ratio of R_n to R_a is harder to see but can be estimated as follows. The reluctance of a cylindrical gap is given by

$$R_a = \frac{1}{2\pi\mu_0 h_a}\ln\frac{r_o}{r_i} \approx \frac{1}{2\pi\mu_0 h_a}\frac{r_o - r_i}{r_i}, \tag{7}$$

where r_i and r_o are the inner and outer radii of the cylindrical air gap width height h_a. The expression to the right of the approximate sign is valid when the width of the gap $d_a = r_o - r_i$ is much smaller than r_i. By neglecting the small difference in radius between the inner yoke and the spacer, and by assuming that its relative permeability is one, the reluctance of the nonmagnetic spaces is $R_n = h_n/(\pi\mu_0 r_i^2)$. Hence, the requirement of $R_n >> R_a$ can be written as $h_n >> d_a r_i/(2h_a)$.

The design is demonstrated on the following example. The design constraints are: two hollow cylinders of Sm_2Co_{17} with an outer diameter of 500 mm and a height of 50 mm, the inner and outer radii of the air gap are 265 mm and 285 mm, the height of each air gap is 100 mm, the outer radius of the magnet (yoke) is 400 mm and its total height is $(600 + d)$ mm, where d denotes the height of the non-magnetic material.

In a first step the radial magnetic field in the centre of the air gap, B_r, as a function of the separation distance d is evaluated. Figure 5 shows the results based on the finite element analysis (FEA). The maximum value is calculated with only the upper or the lower half of the magnet, i.e. $d \to \infty$, $R_n \to \infty$. As the analysis in equation (6), the magnetic flux density decreased quickly when d is getting smaller, which is due to the magnetic reluctance reduction between the upper and lower magnetic circuits. In the example, we use $d = 150$ mm, the magnetic field in the air gap can reach about 91% of the maximum value.

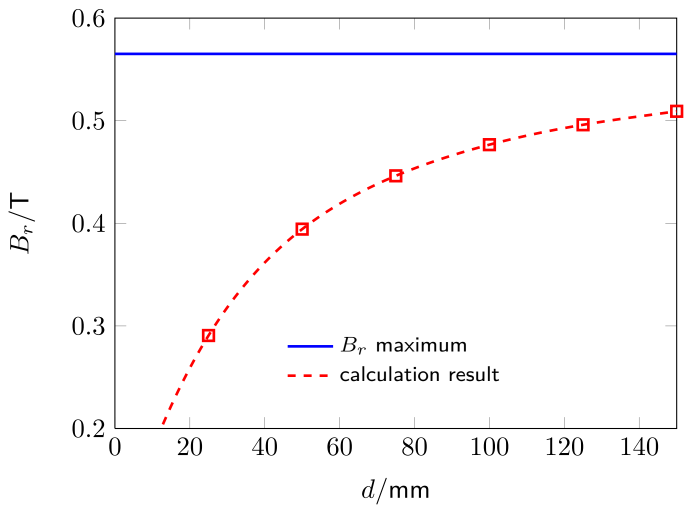

Figure 5: Calculation results of the horizontal magnetic flux density in the air gap, B_r, as a function of the height of the non-magnetic material d.

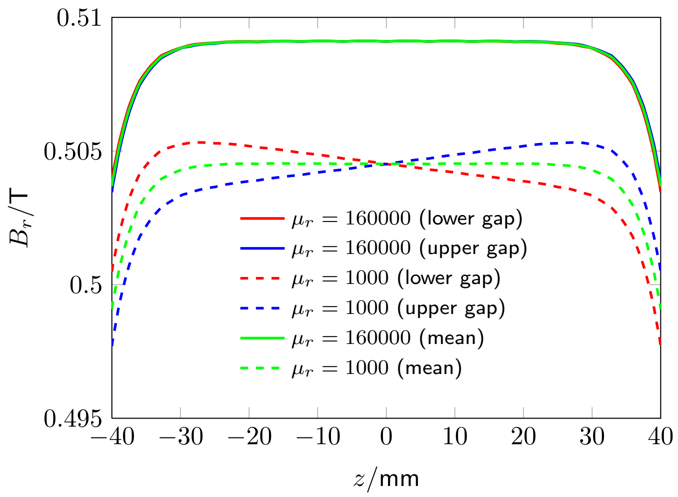

Figure 6: The magnetic profiles in the air gap with different yoke permeabilities. The data represented by the solid lines are calculated using FeNi alloy ($\mu_r \approx 160\,000$). The data shown with the dashed lines are calculated using the permeability of low-carbon steel ($\mu_r \approx 1\,000$).

Note the calculation result shown in figure 5 is with Supra50[1] (50/50FeNi alloy) as the yoke material, which has a relative permeability $\mu_r \approx 160\,000$ [17]. Other materials can be used as well, e.g. low-carbon steel. In general, steel has a lower permeability $\mu_r \approx 1\,000$, which will lead to less flat profiles in both air gaps. Figure 6 presents the magnet profiles with $\mu_r = 160\,000$ and $\mu_r = 1\,000$. It can be seen that with Supra50, the profile in both air gaps is flatter and no further adjustment, e.g. shimming [19], is required. In addition, the magnetic flux density in a magnet that is built using Supra50 as yoke material is about 1% larger compared to one built using steel.

As has been pointed out [29], the BIPM design achieves a very uniform profile, by reducing the pole height of the outer poles compared to the inner poles. The same mechanism works in the new design presented here with one minor difference. In the BIPM design, the gap has up-down symmetry, hence the pole reduction at the top and the bottom of the air gap is the same. Here, the up-down symmetry is broken for each individual gap. Hence, the overhangs of the inner pole are different at both ends of the air gap.

In the example presented above, a flat B_z is obtained when the outer yoke is 2 mm lower at the end facing the magnet and 4 mm lower at the end facing the non-magnetic material. Figure 7 shows the calculation results of $B_z(r, z)$ in the central region of the air gap. It can be seen that rearranging the outer yoke height reduces the spread of B_z by about a factor of 10.

The temperature stabilization of a Kibble balance magnet is also important, because the magnetization of the permanent magnet, e.g. Sm_2Co_{17}, can have a temperature dependence up to several parts in 10^4 per K. In order to avoid temperature control with mK stability, temperature compensation may be applied. The Kibble balance groups in France at LNE (Laboratoire national de métrologie et d' essais) and Switzerland at METAS (Federal Institute of Metrology) [5, 18] presented an efficient approach by inserting a material with a low Curie temperature into the hole in the centre of the magnet. The idea behind this approach is to balance the permanent magnet flux change and the returned flux in the new material by precisely adjusting the thickness of the insert. A similar method can also be applied to the proposed magnet design.

There is a second method to realize the proposed TGTC magnet. As shown in figure 8, the non-magnetic material can be divided into two equivalent parts (upper and lower) and swapped with the two permanent magnets that are then combined into one large disc. The two permanent magnets introduced earlier can be considered as one, and the above analysis remains the same except the designers should readjust the height of the outer yoke, which depends on the position of the two non-magnetic parts (symmetry of the boundary conditions). Note that one merit of the second magnet realization is that thinner top/bottom yoke covers and hence a more compact magnet size can be obtained. Moreover, since the magnet rings are combined into one, the second design may have an additional advantage of less sensitivity to thermal gradients of the magnet system. The inverted magnet with the thinner shield at the outside of the gaps is very similar to a magnet design that was recently proposed by the Kibble balance group at NPL [30]. While, the NPL group arrived at their design by adding shields to the original NPL magnet, we arrived at a similar design by symmetrizing the current response of the BIPM magnet.

[1]Certain commercial equipment, instruments, or materials are identified in this paper in order to specify the experimental procedure adequately. Such identification is not intended to imply recommendation or endorsement by the National Institute of Standards and Technology, the Bureau International des Poids et Mesures, nor is it intended to imply that the materials or equipment identified are necessarily the best available for the purpose

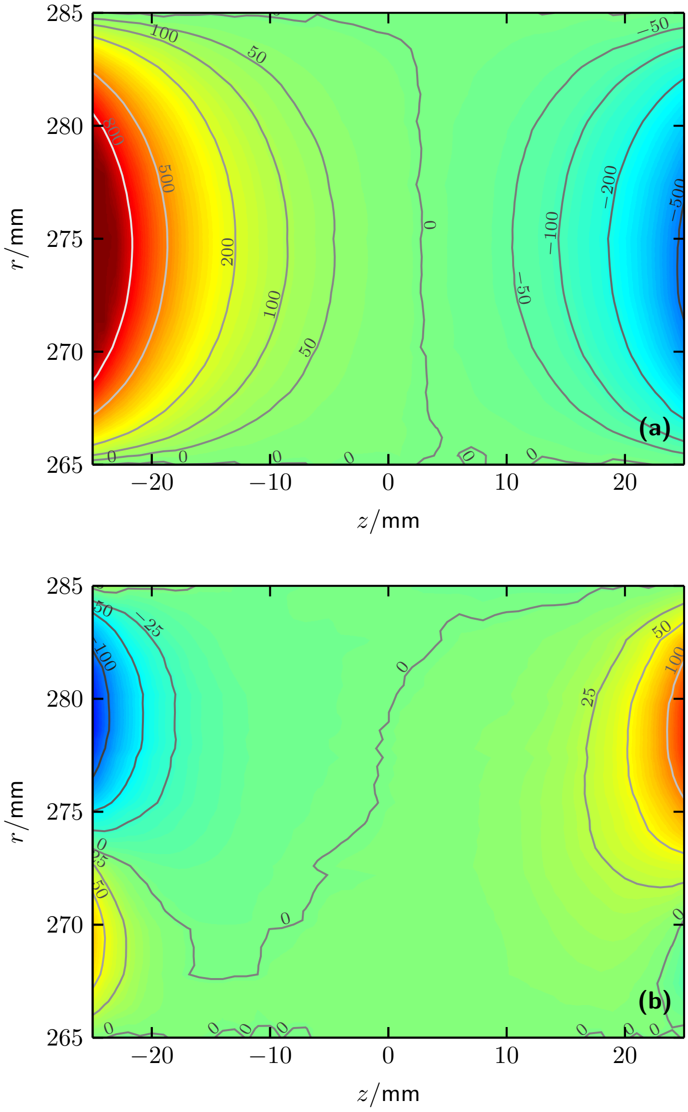

Figure 7: The vertical magnetic flux density B_z distribution in the air gap region, $z \in (-25, 25)\,\mathrm{mm}$, $r \in (265, 285)\,\mathrm{mm}$. The unit of numbers shown on the contour plots is μT. The upper graph shows the B_z distribution when the inner and outer yoke have the same height. The lower graph presents the B_z distribution when the outer yoke height is reduced by 2 mm at the end close to the magnet and 4 mm at the end close to the non-magnetic material.

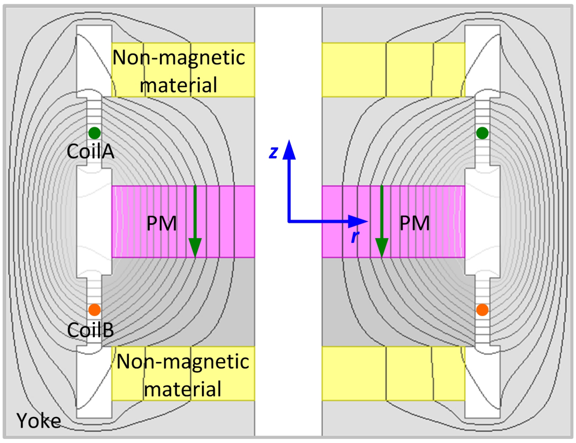

Figure 8: A different construction scheme of the proposed TGTC magnet system. In the structure shown, the permanent magnet and the non-magnetic material are swapped compared to the prior design. The main flux is along the permanent and two air gaps. In order to obtain the same magnetic flux density in the air gap, the height of the permanent magnet should be twice that of the individual permanent magnet in figure 4. Since the top and bottom yoke do not carry much flux, they can be made much thinner than in the previous design.

In summary, the proposed magnet design combines the good shielding performance of the BIPM design with the small dependence of the flux on the coil current of the NPL design. This design is a useful option for future magnet designs or magnet upgrades.

4 Conclusion

The NPL-type magnet can suppress the effect of the coil current on the magnetic flux in the gap by using two coils with opposing currents; however, the shielding is not perfect because of the exposed air gaps. The BIPM design improves the shielding by moving the air gap completely inside the yoke, but the dependence of the magnetic field on the current in the coil is one order of magnitude higher than for the NPL design. Here, a new magnet design is presented that combines both advantages while avoiding the disadvantages of each design. The proposed magnet has good shielding properties and the sensitivity of the magnetic field to the coil current is reduced by one order of magnitude as compared to the BIPM-type, single gap, scheme.

The new design employs two cylindrical magnets and one cylinder made from non-magnetic materials to avoid shorting the magnetic flux. Not all the available flux goes through the gaps housing the coils, but with appropriate dimensions of the non-magnetic material, about 91% of the available flux density can be used. Using high permeability yokes yields exceptional flatness of the two profiles in the upper and lower air gaps. Also, the vertical magnetic flux density component B_z can be well suppressed by optimizing the height of the outer yoke, which should be slightly shorter than the height of the inner yoke. Other techniques for improving the magnet, e.g., temperature compensation, can also be applied to the proposed design.

References

[1] Kibble B P 1976 A measurement of the gyromagnetic ratio of the proton by the strong field method *Atomic Masses and Fundamental Constants 5* pp 545-551

[2] Robinson I A 2011 Towards the redefinition of the kilogram: a measurement of the Planck constant using the NPL Mark II watt balance *Metrologia* **49** 113-56

[3] Sanchez C A *et al* 2014 A determination of Planck's constant using the NRC watt balance *Metrologia* **51** S5-14

[4] Haddad D *et al* 2016 A precise instrument to determine the Planck constant, and the future kilogram *Rev. Sci. Instrum.* **87** 061301

[5] Baumann H *et al* 2013 Design of the new METAS watt balance experiment Mark II *Metrologia* **50** 235-42

[6] Thomas M *et al* 2015 First determination of the Planck constant using the LNE watt balance *Metrologia* **52** 433-43

[7] Fang H *et al* 2013 Status of the BIPM watt balance *IEEE Trans. Instrum. Meas.* **62** 1491-8

[8] Zhang Z *et al* 2014 The joule balance in NIM of China *Metrologia* **51** S25-31

[9] Sutton C M *et al* 2014 A magnet system for the MSL watt balance *Metrologia* **51** S101-6

[10] Kim D *et al* 2014 Design of the KRISS watt balance *Metrologia* **51** S96-100

[11] Ahmedov H 2015 An oscillating magnet watt balance arXiv:1510.01090

[12] Haddad D *et al* 2016 Bridging classical and quantum mechanics *Metrologia* **53** A83-5

[13] Robinson I A *et al* 2016 The watt or Kibble balance: a technique for implementing the new SI definition of the unit of mass *Metrologia* **53** A46-74

[14] Schlamminger S *et al* 2014 Determination of the Planck constant using a watt balance with a superconducting magnet system at the National Institute of Standards and Technology *Metrologia* **51** S15-24

[15] Robinson I A, Kibble B P 2007 An initial measurement of Planck's constant using the NPL Mark II watt balance *Metrologia* **44** 427-40

[16] Stock M 2006 Watt balances and the future of the kilogram *INFOSIM Informative Bulletin of the Inter American Metrology System (November 2006)-OAS* pp 9-13

[17] Li S *et al* 2017 A permanent magnet system for Kibble balances *Metrologia* **54** 775-83

[18] Gournay P *et al* 2005 Magnetic circuit design for the BNM watt balance experiment *IEEE Trans. Instrum. Meas.* **54** 742-5

[19] Seifert F *et al* 2014 Construction, Measurement, Shimming, and Performance of the NIST-4 Magnet System *IEEE Trans. Instrum. Meas.* **63** 3027-38

[20] You Q *et al* 2017 Designing model and optimization of the permanent magnet for joule balance NIM-2 *IEEE Trans. Instrum. Meas.* **66** 1289-96

[21] Li S *et al* 2017 Coil-current effect in Kibble balances: analysis, measurement and optimization, accepted by *Metrologia.*

[22] Lan J *et al* 2012 A compensation method with a standard square wave for precise dc measurement of mutual inductance for Joule balance *IEEE Trans. Instrum. Meas.* **61** 2524-32

[23] Zhang Z *et al* 2015 Coils and the Electromagnet Used in the Joule Balance at the NIM *IEEE Trans. Instrum. Meas.* **64** 1539-45

[24] Li S *et al* 2013 Nonlinear magnetic error evaluation of a two-mode watt balance experiment *Metrologia* **50** 482-89

[25] Li S *et al* 2014 A nonlinearity in permanent-magnet systems used in watt balances *Metrologia* **51** 394-401

[26] Haddad D *et al* 2017 Measurement of the Planck constant at the National Institute of Standards and Technology from 2015 to 2017 *Metrologia* **54** 633-41

[27] Wood B M *et al* 2017 A summary of the Planck constant determinations using the NRC Kibble balance *Metrologia* **54** 399-409

[28] Davis R *et al* 2003 Magnetic properties of weights, their measurements and magnetic interactions between weights and balances *Metrologia* **40** 339-55

[29] Li S, Schlamminger S 2017 Two simple modifications to improve the magnetic field profile in radial magnetic systems *Meas. Sci. Technol.* **28** 107001

[30] Oral presentation by Robinson I A at WBTM 2017 in Bejing, China.